

Functional Optical Detection Based on pH Dependent Fluorescence Lifetime

Israel Gannot, PhD,^{1,2*} Izhar Ron, MSc,¹ Farid Hekmat, BSc,² Victor Chernomordik, PhD,¹ and Amir Gandjbakhche, PhD¹

¹*Lasers and Optics in Medicine Laboratory, Department of Biomedical Engineering, Faculty of Engineering Tel-Aviv University, Tel-Aviv 69978, Israel*

²*Laboratory of Integrative and Medical Biophysics, National Institutes of Health, Bethesda, Maryland 20892*

Background and Objectives: Detection of possible alterations of physiological parameters (e.g., pH and temperature), resulting from malignant transformation of initially healthy tissue, can be a powerful diagnostic tool for earlier cancer detection. Such variations can be observed by comparing these parameters with those of healthy tissue surrounding the abnormality. Time-resolved spectroscopy of specifically targeted fluorescent labeled antibodies can be sensitive to such variations and provide a high resolution functional image of the region of interest. The goal of this study was to establish a forward experimental setup for calibration of the lifetime dependencies of near-IR fluorescent dyes on physiological parameters, and to develop analytical solutions, taking into account the effects of light propagation in turbid media (e.g., tissue), that was able to extract an original lifetime fluorescence signal from time-of-flight intensity distributions, measured in vivo from a deeply embedded live organ for further analysis.

Study Design/Materials and Methods: Tissue-like phantoms with embedded fluorescent dyes and background optical properties simulating those of live tissues were designed and created. Fluorescence decay curves were measured for different fluorophore positions, and pH values. Those measurements were made with a system based on a time-correlated single photon counting (TCSPC) instrument and a tunable femtosecond Ti-Sapphire system built by our group.

Results: Decay curves were recorded for fluorophore depths of up to 5 mm and source-detector separation of 7 mm. It was shown that a forward model, based on the random walk theory, adequately described the experimental data. Measured pH dependencies of the fluorescence lifetime were characterized for two different dyes.

Conclusions: Good correlation between experimental data and predictions of the theoretical model allows the use of close-form analytical solutions to separate the effects of photon time delays due to multiple scattering in tissues from the original intensity fluorescence time decay curve, determined by the fluorophore itself and its immediate surroundings. It is the latter dependence that can be diagnostically important. Experimentally obtained scaling between lifetime and a parameter of interest can be used in vivo to obtain a map of physiological parameter changes

which can serve as a base for an in vivo specific diagnostic system. *Lasers Surg. Med.* 35:342–348, 2004.

© 2004 Wiley-Liss, Inc.

Key words: minimal invasive optical detection; time resolved fluorescence; physiological parameters in tissue

INTRODUCTION

Optical imaging techniques have been widely investigated over the last decade for biomedical diagnostic applications. Some aspects of optical spectroscopy are being considered in order to overcome constraints arising from specific biological tissues. One such consideration is to use a light source that emits in the near-IR region and fluorescent dyes that absorb and emit in this spectral range, where tissue absorption is relatively low, thus allowing for deeper light penetration within the tissue. Another approach is aimed toward detecting time-resolved characteristics of the fluorescence, rather than its intensity, since they may provide additional information about environmental conditions in the immediate vicinity of a fluorescent probe. Our goal is to apply fluorescence lifetime imaging of specifically targeted lifetime-based fluorescent probes to map physiological parameters in vivo. Such an approach is a promising tool for early, minimally invasive detection of diseases, primarily cancer.

Many studies have related alterations of physiological parameters to the early stages of tumor development. The extracellular pH (pH_e) in a tumor microenvironment tends to exhibit a lower value than the surrounding normal tissue, a phenomenon that is sometimes referred to as “acidosis.” It is considered to originate from a high metabolic rate in a rapidly growing tumor, sometimes accompanied by insufficient disposal of waste products [1,2]. The pH_e value in many solid tumors is low and can

*Correspondence to: Dr. Israel Gannot, PhD, Lasers and Optics in Medicine Laboratory, Department of Biomedical Engineering, Faculty of Engineering Tel-Aviv University, Tel-Aviv 69978, Israel. E-mail: gannoti@mail.nih.gov

Accepted 11 August 2004

Published online in Wiley InterScience (www.interscience.wiley.com).

DOI 10.1002/lsm.20101

drop to 5.6, in contrast to the pH_e range of 7.2–7.6 for normal tissue [3]. Measurements of pH_e were performed both in animal models and various human tumors [4,5]. In these studies, a variety of malignant tumors were analyzed in vivo, and pH_e was measured using microelectrodes. Experimental findings clearly indicated a positive correlation between the tumor size and the decrease in pH_e . However, the decrease in pH_e was observed even in small tumors.

Lifetime-based sensors for these parameters have been investigated for other spectral ranges [6–8]. The change in pH may change the luminescence decay time (e.g., decrease or increase the lifetime) and is usually determined by the chemical functional groups bound to the dye molecule (rather than by the chromophore itself). Collisional quenching by protons usually results in a shortened decay time.

Fluorescence lifetime imaging attracts growing interest in the field of molecular, cellular, and tissue imaging. This is because the lifetime is an intrinsic parameter of the fluorescent probe, and, being independent of the probe concentration and possible photobleaching, it is sensitive to changes in the immediate environment of the probe. Distinguishing a non-malignant tissue from a malignant one by means of fluorescence lifetime measurement includes tracing conformational changes in specific molecules that are labeled with a fluorescent dye and are involved in signal transduction processes in cancerous cells [9], quantifying changes in tissue oxygenation [10], observing longer lifetimes of an exogenous dye in cancerous regions of the tissue [11,12] and histopathological assessment of breast cancer tissue by measuring the decay of tissue autofluorescence. The main challenge in lifetime imaging lies in the analysis of the recorded data. Complications arise at depths greater than 1 mm, where photons enter a diffusion-like state with large dispersion in their path-lengths [13–16]. Since the fluorescent decay curve, collected from deep tissue structures, depends not only on the location, size, and lifetime of the fluorophore, but also on the scattering and absorption coefficients of the tissue at both excitation and emission wavelengths, it is necessary to describe the statistics of photon path-lengths that depend on all of these parameters. For time-resolved fluorescent measurements, a closed-form, analytical solution for diffuse media has not been developed. For lifetime imaging purposes, Sevick-Muraca et al. [17] have designed numerical methods, including finite element models to devise inverse algorithms based on local differential equations of the diffusion approximation to transport theory. Mycek et al. [18] described a Monte Carlo model that simulates time-resolved fluorescence propagation in semi-infinite turbid medium, and showed scattering-induced changes in fluorescence lifetime with respect to, among others, spatial separation between the source and detector.

In this article, the first steps in the development of a new method are presented for early, minimally invasive diagnosis of pH changes by means of fluorescence lifetime measurements of specifically targeted exogenous fluorescent probes. The approach is based on the immune cell infiltrate profile of induced squamous cell carcinoma

(SqCC) in mice, in different stages of lesions [19,20]. In the current study, the aim is to create a pH values map, derived from lifetime value matrices of the tumor area and the scaling between the lifetime and the physiological value of interest.

MATERIALS

Optical Phantoms

Two materials were used as optical phantoms to simulate the effect of turbid media (such as tissue) on the excitation and fluorescent photons. Agarose-based gels were prepared by dissolving 0.8 g agarose (SeaKem HE Agarose, FMC Bioproducts, Cambrex Corporation, NJ) in 36.6 ml phosphate-buffer saline (PBS) (J.T. Baker, Catalog No. 5656) while boiling and stirring the solution for 5 minutes. After cooling to 70°C, 3.4 ml of Intralipid (Intralipid 20%, Pharmacia and Upjohn, Catalog No. 406563A) was added to the solution and spread uniformly by shaking the tube. For preparation of phantoms with different pH values, fixed pH buffer solutions (Buffer Concentrate Series, Merck, and 565× Buffer Solution Series, J.T. Baker) were used as the dissolving media instead of PBS. A complete system for sensing pH (designed also for in vivo experiments) consisted of 100 μm glass tip pH-microelectrodes (PH100, Unisense) and the corresponding meters (PHM210, Radiometer Analytical). The analog signals were output through an A/D converter (ADC101, Pico Technology) to a PC and displayed by software (PicoScope, Pico Technology). The second substance used for phantoms was Delrin™, available as white cylindrical plastic slabs, with small wells on the surface where up to 5 μl of fluorescent dye dissolved in a buffer solution could be loaded. The optical properties of each sample were measured by an integrating sphere system (LabSphere). The measured diffuse reflectance and diffuse transmittance were input to a random walk based algorithm together with the sample's thickness, and the reduced scattering and absorption coefficients were calculated.

Fluorescent Dyes

Fluorescent dyes IRD38 and IRD41 (Li-Cor, Inc.) were used, with absorption peaks at 778 and 786 nm, and emission peaks at 806 and 812 nm, respectively. The quantum efficiencies of the dyes were 34.5 and 14.1% in methanol, respectively, and the natural lifetime was 600 picoseconds according to the manufacturer. The dyes were attached to the amino groups of microspheres (PA06N, 5–9.9 μm , Bangs Laboratories, Inc.) in order to prevent diffusion of the dye within the phantom. The phantoms were prepared as described above and the microsphere conjugated fluorescent dyes were injected into a specific location on the surface of the gel. Then the phantom was covered with slabs of the same optical properties but different thicknesses to simulate different depths.

METHODS

In order to measure the fluorescent decay curve for the localized fluorescent marker, a TCSPC fluorescent lifetime

measurement system was established. The sample was excited with 80 MHz repeated pulses from a mode-locked, Ti:Sapphire femtosecond laser (Tsunami, Spectra-Physics Lasers), pumped by a 5 W, 532 nm all-solid-state laser (Millenia Vs., Spectra-Physics Lasers). The excitation was tuned to the absorption peak wavelength of the investigated dye. The excitation beam was split to a fast photodiode (PHD-400, Becker & Hickl GmbH) for signal synchronization and directed to the sample area, by a reflecting mirror. The sample was placed on an XYZ micrometer stage. Fluorescent photons were collected by a lens, and encountered a bandpass filter with a cut-on at 790 nm (Omega Filters, Custom Design No. 835BP70) and a single-grating monochromator (CM110, CVI Laser Corporation) coupled to the entrance of the fast photomultiplier tube (PMT) head (H7422P-50, Hamamatsu) with a minimal rise time of 200 picoseconds and FWHM down to 240 picoseconds. The output from the PMT was further amplified by a gain amplifier with a maximum of 26 dB (HFAC-26, Becker & Hickl GmbH). Control of the cooling current and gain voltage of the PMT were integrated on a PCI bus (DCC-100, Becker & Hickl GmbH), as were the TCSPC electronics (SPC-730 TCSPC Module, Becker & Hickl GmbH) with the SYNC signal arriving from the photodiode and from the constant fraction discriminator (CFD) signal from the PMT.

The experimental setup scheme is shown in Figure 1. For a single decay curve, photons were collected up to 45,000 counts at the peak. The instrumental impulse response was measured by folding the laser pulse into the detection channels using a mirror positioned in place of the sample. Measured fluorescent intensity decay curve was a convolution of this instrumental impulse response function and actual decay dependence. Thus, the actual decay dependence could be extracted by a deconvolution procedure (see “Results and Discussion” for theoretical analysis) from the measured decay curve.

Fluorescence intensity decay was measured for a localized fluorescent marker (1 μL of IRD38-microbeads from a stock of 8×10^8 beads/mL) in an agarose phantom, prepared in different pH buffer solutions to simulate variations in pH in the vicinity of the fluorophore.

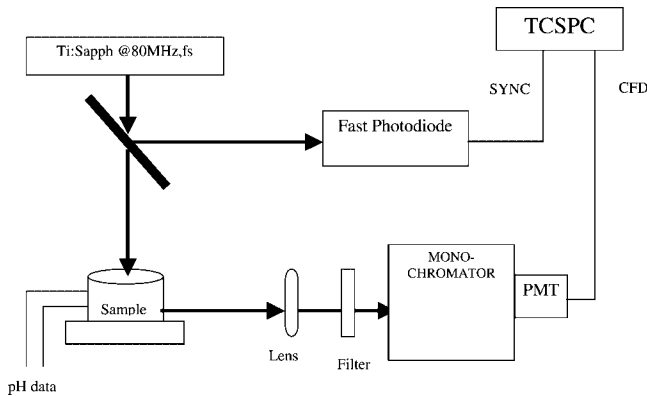


Fig. 1. Experimental setup.

Different depths of the fluorophore inside the highly scattering medium were modeled by placing tissue-like turbid slabs of known thicknesses over the fluorescent inclusion (as explained in “Materials”). Increasing source-detector separation was realized by a simultaneous shift of the sample by a given distance and detection point by twice that distance, providing that the fluorophore was halfway between the excitation light entry and the exit point of detected emission photons. Measurements have been also taken for the case when the source-detector separation was twice the depth of fluorophore.

Random Walk Model of Predicted Intensity Decay, As a Tool to Extract Fluorescence Lifetime Variations Inside Turbid Media

Random walk theory was used to create a forward model that allows the separation of an intrinsic lifetime component from the path-length dispersion for time-resolved measurements in turbid media [21]. It was shown that, if the intrinsic fluorescence lifetime equaled $\langle \Delta t \rangle$, then the probability that an emitted photon arrived at the detector at time t after the excitation pulse was:

$$\gamma(t) = \frac{\mu_{af}}{\mu_{si}'} \Phi \left[W_t - \langle \Delta t \rangle \frac{dW}{dt} \right] \quad (1)$$

where W_t , corresponding to a point-spread function, was given by

$$W_t = \Phi \frac{\mu_{af}}{\mu_{sf}'} [h(\alpha_-, \beta_-) - h(\alpha_-, \beta_+) - h(\alpha_+, \beta_-) + h(\alpha_+, \beta_+)] \quad (2)$$

$$h(\alpha, \beta) = \frac{\sqrt{\alpha} + \sqrt{\beta}}{(ct\sqrt{\mu_{si}'\mu_{se}'})^{3/2} \sqrt{\pi\alpha\beta}} \exp \left[-\frac{(\sqrt{\alpha} + \sqrt{\beta})^2}{ct\sqrt{\mu_{si}'\mu_{se}'}} - ct\mu_a \right] \quad (3)$$

$$\alpha_{\pm} = \frac{3}{4} \left[x_f^2 + y_f^2 + \left(z_f \pm \frac{\sqrt{2}}{\mu_{si}'} \right)^2 \right] \mu_{si}'^2 \quad (4)$$

and

$$\beta_{\pm} = \frac{3}{4} \left[(\bar{x}_f - x)^2 + (\bar{y}_f - y)^2 + \left(\bar{z}_f + \frac{\sqrt{2}}{\mu_{se}'} \pm \frac{\sqrt{2}}{\mu_{se}'} \right)^2 \right] \mu_{se}'^2 \quad (5)$$

Here, the origin of the coordinate system (0,0,0) was placed at the entry point for the incident photon, and coordinates of the fluorescent site and the detector were $(\bar{x}_f, \bar{y}_f, \bar{z}_f)$ and $(\bar{x}, \bar{y}, \bar{z})$, respectively. The optical parameters, $\mu_{s'}$ and μ_a , were the transport-corrected scattering coefficient and absorption coefficients of the background, respectively. The subscripts i and e stood for incident and emitted light, respectively. μ_{sf}' and μ_{af}' were the optical characteristics of the fluorescent site. The parameter Φ (so-called quantum efficiency) was the probability that an excited fluorophore would emit a fluorescent photon.

Equation (1) shows that the effect of the fluorescence lifetime delay was proportional to the time-derivative of the point-spread function. It should be noted that Equation (1) was derived under the simplifying assumption that $\langle \Delta t \rangle$ was small compared to a mean photon transit time from the source to the fluorophore and then to the detector. In fact, this assumption could be considered as a limitation on experimental set-ups (lifetime of the fluorescent agent, its depth, source-detector separation and optical properties of the turbid medium) that can be analyzed within such theoretical framework [21]. It has been shown from Equation (1) that the time-resolved fluorescence contrast between two measurements taken on the surface of scattering media could be expressed as follows [21]:

$$C = \frac{(\langle \tau \rangle - \tau_s) dW_t}{p_t dt} \quad (6)$$

Where $\langle \tau \rangle$ was the mean lifetime of the background tissue and τ_s was the perturbed lifetime inside an abnormality (e.g., potential tumor), and p_t was the probability that a photon would arrive at the detector, after visiting the site of the fluorophore in the absence of any fluorescent reemission. The value of p_t could be estimated from intensity measurements at the excitation wavelength. The last factor, dW_t/dt , strongly depends on geometry of the experimental set-up (relative positions of the source, detector, and fluorophore).

RESULTS AND DISCUSSION

The effect of multiple scattering and absorption of the background at the excitation wavelength could be characterized by broadening the impulse response (as compared to the initial laser pulse entering the emission channel) after transmission through phantom slabs of increasing thickness (Fig. 2). The setup for measuring the effect of source-detector separation accounts for the path-lengths of both the excitation and emitted photons, with the fluorophore centered within this distance is shown in Figure 3. Both the delay in the rise time of the signal and the delay in

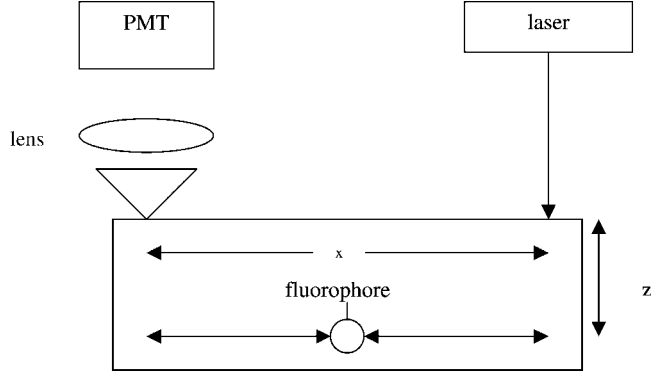


Fig. 3. Experimental coordinates scheme.

decay increased with increasing distance between the source entrance and photon exit toward the detector (Fig. 4) in a relatively easy to quantify manner. This data was acquired for IRD38-microspheres complexes regardless of the other parameters in order to extract the pattern of delay in photon arrival time. The effect of the second component of the fluorophore's position, its depth, was measured by covering the fluorophore's inclusion, located on the surface of the phantom, with phantom slabs of known thickness thus simulating different depths of the fluorophore. A set of decay curves for IRD38-microspheres complexes embedded in different depths is shown in Figure 5. The photons at the excitation wavelength were also shown to disperse (in space and consequently in time). They dispersed less than when traveling a lateral distance, and the dispersion of the emitted photons through this depth should be compared to what was measured for the lateral distance (source-detector separation), in order to distinguish between the two components. The combined effect was measured for source-detector distances that were twice the depth component, and is shown in Figure 6.

The next step was to look for a dependence of the dye's decay time on the pH. In order to do so, optical phantoms

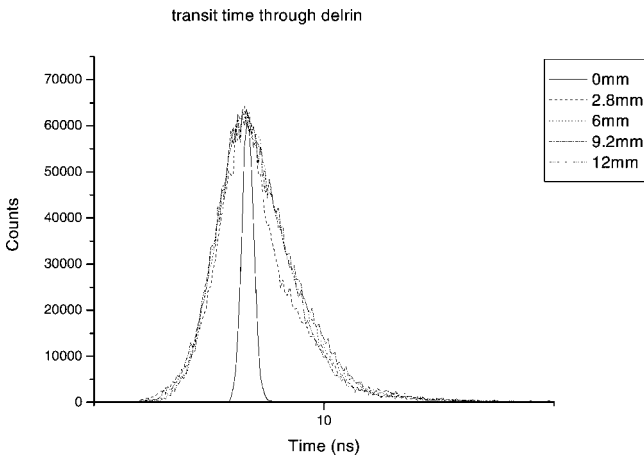


Fig. 2. Transit time of excitation photons through delrin media.

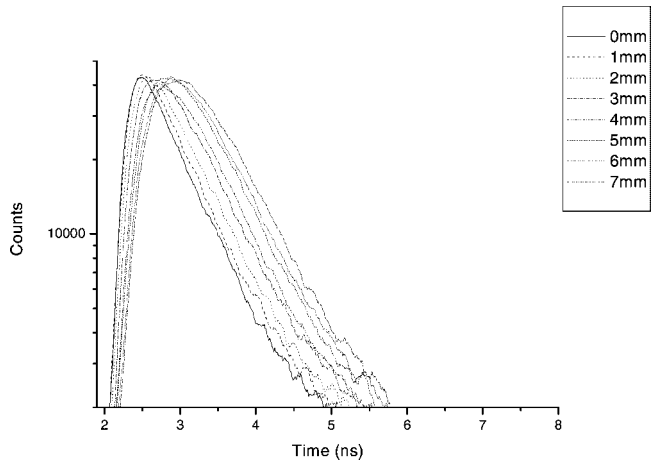


Fig. 4. Source-detector separation at pH 7.

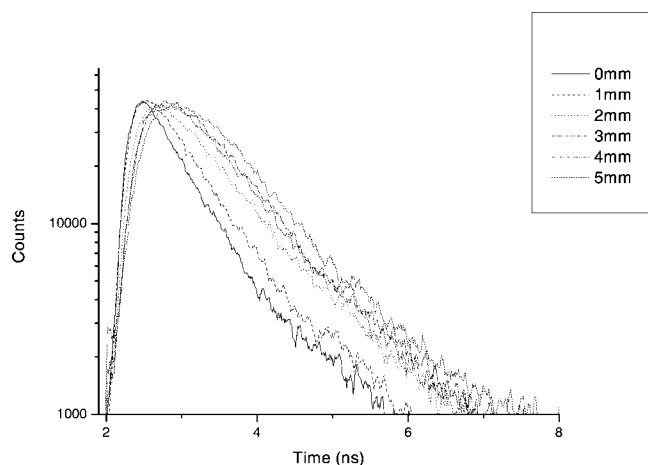


Fig. 5. Depth variation at pH 7.

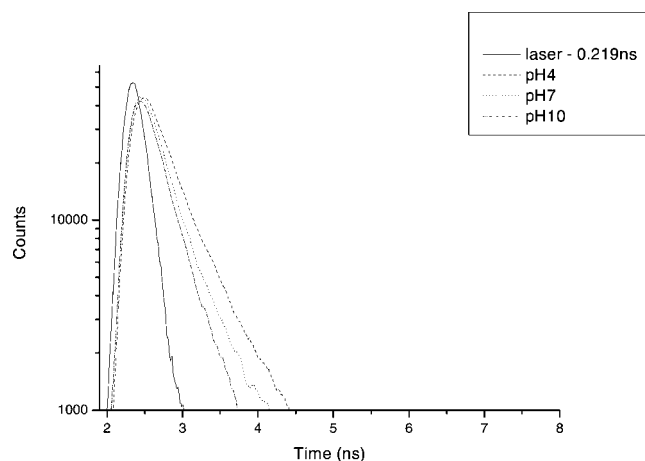


Fig. 7. IRD38-beads at different pH in agarose.

were prepared with fixed chosen pH values (in the range of pH 4–10) and the dye-microsphere complex was embedded on the surface of the sample. The measurements shown here were taken for a broad pH range since no pronounced effect of the pH on fluorescent lifetime was observed from the preliminary measurements. The decay curves of IRD38-microsphere complexes in different pH phantoms are shown in Figure 7. The optical properties of the agarose-based phantom seemed to be affected by the alkalinity of the preparation buffer solution. Therefore, the same measurements were also taken for samples of dye-microsphere complexes dissolved in a buffer and loaded in a well in a DelrinTM phantom, keeping the same optical properties regardless of the pH of the sample. These results are shown in Figure 8.

Data analysis was performed in two steps: data deconvolution, using the known instrumental response of the system, and fitting the corrected data to the theoretical forward model for fluorescence intensity decay, observed

through the turbid medium described in “Results and Discussion.”

First, the raw time-resolved intensity distributions were corrected for the instrumental impulse response function which was responsible for the broadening of observed intensity distributions. This function, determined by the optical setup and non-ideal detection components, had been estimated experimentally in advance, as described in “Methods.” The measured time-resolved signal was deconvolved, using conventional procedures, based on the Fast Fourier Transform (FFT) of both the signal and instrumental impulse responses, accompanied by filtering out the high frequency noise [22]. The ratio of Fourier components of the signal and instrumental response frequency components was calculated, and inverse FFT was performed to get the de-convoluted signal. It should be noted that small high frequency oscillations, seen at the long-time tails of the deconvolved intensity distributions were actually artifacts of the deconvolution procedure. They resulted

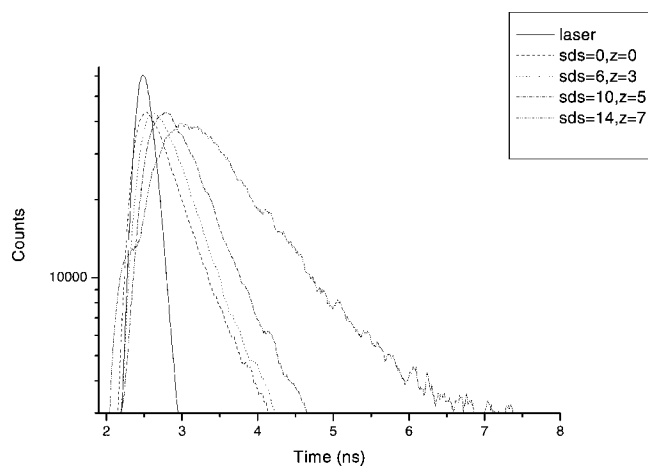


Fig. 6. Combination of source-detector separation and depth at pH 7.

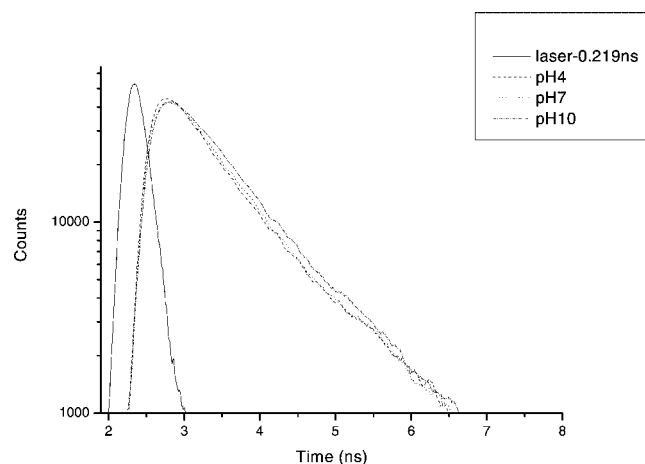


Fig. 8. IRD41-beads at different pH in delrin.

from enhancement of the leftover high frequency noise in the measured distributions due to small values of the high frequency components of the response function. However, these oscillations didn't change the results of the fitting procedure that smoothed the data. This procedure allowed the separation of contributions intrinsic to the fluorescent event (lifetime) and those that originated from the propagation effects in the highly scattering medium (time delay).

To compare corrected experimental data and model predictions, a MATLAB code was written that simulated an intensity decay curve, based on the analytical solution described in "Results and Discussion." This forward model, calculated for reasonable values of relevant parameters, was then used as the starting point for comparison with the experimental data. This was done using the Curve Fitting Toolbox from MATLAB. This toolbox allowed for choosing any number of fitting parameters while setting others constant and then obtaining a best fit to the deconvolved experimental data. The curve fitting application worked best when only a few parameters were isolated. Besides absorption and scattering coefficients, the position of the fluorophore (depth and source-detector separation), the known natural lifetime, an overall scaling coefficient and time-scaling constant were added to the code to better fit the data. This simulation was compared to the deconvolved experimental data. The theory was tested for correctness by matching the raw data to the forward model using the calculated parameter from the curve-fitting application for a single changed parameter (e.g., depth) with all other parameters held constant. The results of correlations between computational simulations and experimental data (using IRD38-microspheres complexes) for pH 7 at different fluorophore depths are shown in Figure 9 (3 mm depth) and Figure 10 (5 mm depth) using normalized intensities. The calculated scattering coefficients were 0.993 and 0.979 mm^{-1} , and the absorption coefficients were 0.133 and 0.135 mm^{-1} , respectively. For both cases, values of

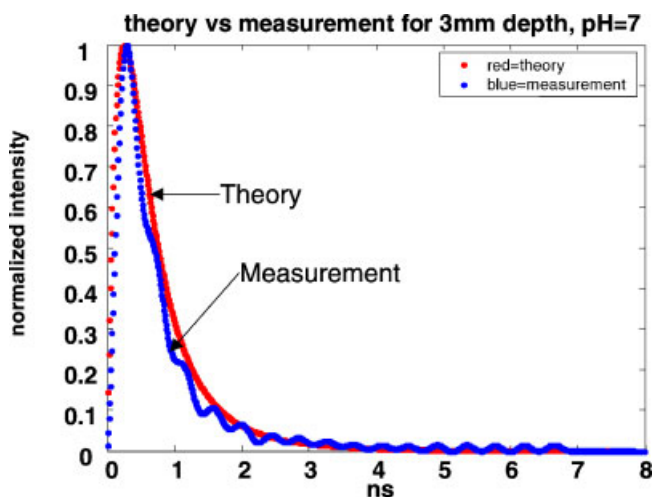


Fig. 9. Correlation with theory for pH7 and 3 mm depth. [Figure can be viewed in color online via www.interscience.wiley.com.]

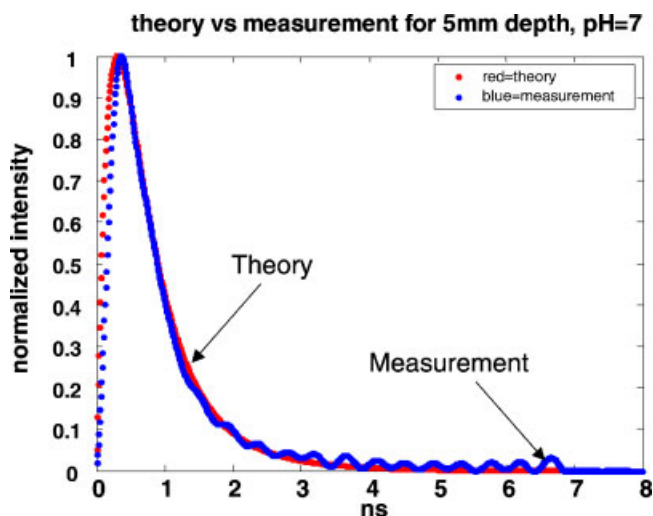


Fig. 10. Correlation with theory for pH7 and 5 mm depth. [Figure can be viewed in color online via www.interscience.wiley.com.]

optical coefficients were reasonable; moreover, the discrepancies in estimated parameters were within 1.5% error. Figure 11 presents a comparison of normalized intensities at a constant depth of 5 mm for varying pH. A scattering coefficient of 1 mm^{-1} and an absorption coefficient of 0.01 mm^{-1} were assumed for the forward model.

SUMMARY

A TCSPC fluorescence lifetime measurement system was established that was suitable for measuring the fluorescence lifetime in the experimental context of the application. Data was collected regarding the behavior of decay shapes with respect to the position of the fluorophore and the surrounding pH value, and correlated with theoretical simulations, where satisfying results from this step should

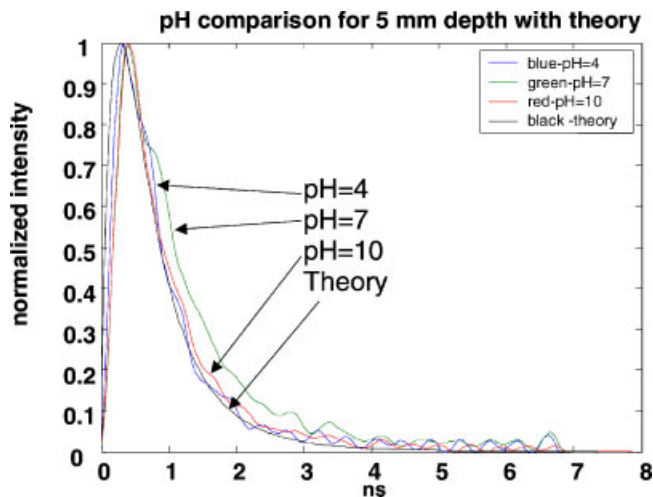


Fig. 11. Correlation with theory for 5 mm depth and different pH. [Figure can be viewed in color online via www.interscience.wiley.com.]

be the basis for the analytical solutions of the inverse problem. The next steps are to scan a sample in the XY plane and synchronize the scanning coordinates with the TCSPC system, thus obtaining a 2D lifetime map from every sample. This 2D map will then be translated into a pH values map according to scaling measurements. In this map (matrix) the source-detector separation will be known for each pixel (from synchronizing the scanning program with the decay curve recording program), and only the depth of fluorophore will have to be extracted. After fixing for depth and source detector separation, the pH is the only parameter that affects the decay time change. Once the first analytical solutions are ready to be implemented, in vivo measurements will take place and the results will be compared with histopathological analysis.

ACKNOWLEDGMENTS

Mr. Izhar Ron would like to thank the American Society for Laser Medicine and Surgery for the student summer research grant.

REFERENCES

- Boyer MJ, Tannock IF. Regulation of Intracellular pH in tumor-cell lines—Influence of microenvironmental conditions. *Cancer Res* 1992;52(16):4441–4447.
- Wahl ML, Pooler PM, Briand P, Leeper DB, Owen CS. Intracellular pH regulation in a nonmalignant and a derived malignant human breast cell line. *J Cell Physiol* 2000;183(3):373–380.
- Griffiths JR. Are cancer-cells acidic. *Br J Cancer* 1991;64(3):425–427.
- Engin K, Leeper DB, Cater JR, Thistlethwaite AJ, Tupchong L, McFarlane JD. Extracellular pH distribution in human tumors. *Int J Hyperthermia* 1995;11(2):211–216.
- Kallinowski F, Vaupel P. pH distributions in spontaneous and isografted rat-tumors. *Br J Cancer* 1988;58(3):314–321.
- Andersson RM, Carlsson K, Liljeborg A, Brismar H. Characterization of probe binding and comparison of its influence on fluorescence lifetime of two pH-sensitive benzo c xanthene dyes using intensity-modulated multiple-wavelength scanning technique. *Anal Biochem* 2000;283(1):104–110.
- Draxler S, Lippitsch ME. pH sensors using fluorescence decay time. *Sensors and Actuators B-Chemical* 1995;29(1–3):199–203.
- Lin HJ, Szmajnski H, Lakowicz JR. Lifetime-based pH sensors: Indicators for acidic environments. *Anal Biochem* 1999;269(1):162–167.
- Gadella TWJ, Jovin TM. Oligomerization of epidermal growth-factor receptors on A431 cells studied by time-resolved fluorescence imaging microscopy—A stereochemical model for tyrosine kinase receptor activation. *J Cell Biol* 1995;129(6):1543–1558.
- Bambot SB, Rao G, Romauld M, Carter GM, Sipior J, Terpetchnig E, Lakowicz JR. Sensing oxygen through skin using a red diode-laser and fluorescence lifetimes. *Biosens Bioelectron* 1995;10(6–7):643–652.
- Cubeddu R, Pifferi A, Taroni P, Valentini G, Canti G. Tumor detection in mice by measurement of fluorescence decay time matrices. *Opt Lett* 1995;20(24):2553–2555.
- Cubeddu R, Comelli D, D'Andrea C, Taroni P, Valentini G. Time-resolved fluorescence imaging in biology and medicine. *J Phys D Appl Phys* 2002;35(9):R61–R76.
- Bonner RF, Nossal R, Havlin S, Weiss GH. Model for Photon Migration in Turbid Biological Media. *J Opt Soc Am A Opt Image Sci Vis* 1987;4(3):423–432.
- Gandjbakhche AH, Nossal R, Bonner RF. Resolution limits for optical transillumination of abnormalities deeply embedded in tissues. *Med Phys* 1994;21(2):185–191.
- Moon JA, Reintjes J. Image-resolution by use of multiply scattered-light. *Optics Lett* 1994;19(8):521–523.
- Gandjbakhche AH, Weiss GH. Random walk and diffusion-like models of photon migration in turbid media. In: Wolf E, editor. *Progress in optics XXXIV*. Amsterdam: Elsevier Science B.V; 1995. pp 335–402.
- Paithankar DY, Sevick-Muraca EM. Fluorescence lifetime imaging with frequency-domain photon migration measurement. In: Sevick-Muraca E, Benaron D, editors. *Biomedical Optical Spectroscopy and Diagnostics meeting proceeding*, March, Orlando: Optical Society of America; 1996. pp 184–194.
- Vishwanath K, Pogue B, Mycek MA. Quantitative fluorescence lifetime spectroscopy in turbid media: Comparison of theoretical, experimental and computational methods. *Phys Med Biol* 2002;47(18):3387–3405.
- Gannot G, Gannot I, Vered H, Buchner A, Keisari Y. Increase in immune cell infiltration with progression of oral epithelium from hyperkeratosis to dysplasia and carcinoma. *Br J Cancer* 2002;86(9):1444–1448.
- Gannot I, Garashi A, Gannot G, Chernomordik V, Gandjbakhche A. In vivo quantitative three-dimensional localization of tumor labeled with exogenous specific fluorescent markers. *Appl Opt* 2003;42(16):3073–3080.
- Hattery D, Chernomordik V, Loew M, Gannot I, Gandjbakhche A. Analytical solutions for time-resolved fluorescence lifetime imaging in a turbid medium such as tissue. *J Opt Soc Am A Opt Image Sci Vis* 2001;18(7):1523–1530.
- Press W, Teukolsky S, Vetterling W, Flannery B. Numerical recipes in C: The art of scientific computing. New York: Cambridge University Press; 1992.